The transition from 2G to 3G-feedstocks enabled efficient production of fuels and chemicals

Downloaded from: https://research.chalmers.se, 2025-12-04 22:45 UTC

Citation for the original published paper (version of record):
Wang, K., Su, C., Bi, H. et al (2024). The transition from 2G to 3G-feedstocks enabled efficient production of fuels and chemicals. Green Energy and Environment, 9(11): 1759-1770. http://dx.doi.org/10.1016/j.gee.2023.11.004

N.B. When citing this work, cite the original published paper.

research.chalmers.se offers the possibility of retrieving research publications produced at Chalmers University of Technology. It covers all kind of research output: articles, dissertations, conference papers, reports etc. since 2004. research.chalmers.se is administrated and maintained by Chalmers Library

(article starts on next page)

Available online at www.sciencedirect.com

ScienceDirect

Green Energy & Environment xxx (xxxx) xxx

www.keaipublishing.com/gee

Research Paper

The transition from 2G to 3G-feedstocks enabled efficient production of fuels and chemicals

Kai Wang [a,b], Changsheng Su [a,b], Haoran Bi [a,b], Changwei Zhang [a,b], Di Cai [a,b], Yanhui Liu [a,b], Meng Wang [a,b], Biqiang Chen [a,b], Jens Nielsen [a,c], Zihe Liu [a,b,*], Tianwei Tan [a,b,*]

[a] *College of Life Science and Technology, Beijing University of Chemical Technology, Beijing Advanced Innovation Center for Soft Matter Science and Engineering, No. 15 North 3rd Ring Rd East, Beijing, 100029, China*

[b] *National Energy R&D Center for Biorefnery, Beijing Key Lab of Bioprocess, Beijing University of Chemical Technology, No. 15 North 3rd Ring Rd East, Beijing, 100029, China*

[c] *Department of Life Sciences, Chalmers University of Technology, Gothenburg, SE41296, Sweden*

Received 25 August 2023; revised 12 November 2023; accepted 20 November 2023
Available online ■ ■ ■

Abstract

For decades micoorganisms have been engineered for the utilization of lignocellulose-based second-generation (2G) feedstocks, but with the concerns of increased levels of atmospheric CO_2 causing global warming there is an emergent need to transition from the utilization of 2G feedstocks to third-generation (3G) feedstocks such as CO_2 and its derivatives. Here, we established a yeast platform that is capable of simultaneously converting 2G and 3G feedstocks into bulk and value-added chemicals. We demonstrated that by adopting 3G substrates such as CO_2 and formate, the conversion of 2G feedstocks could be substantially improved. Specifically, formate could provide reducing power and energy for xylose conversion into valuable chemicals. Simultaneously, it can form a concentrated CO_2 pool inside the cell, providing thermodynamically and kinetically favoured amounts of precursors for CO_2 fixation pathways, e.g. the Calvin–Benson–Bassham (CBB) cycle. Furthermore, we demonstrated that formate could directly be utilized as a carbon source by yeast to synthesize endogenous amino acids. The engineered strain achieved a one-carbon (C1) assimilation efficiency of 9.2 %, which was the highest efficiency observed in the co-utilization of 2G and 3G feedstocks. We applied this strategy for productions of both bulk and value-added chemicals, including ethanol, free fatty acids (FFAs), and longifolene, resulting in yield enhancements of 18.4 %, 49.0 %, and ~100 %, respectively. The strategy demonstrated here for co-utilization of 2G and 3G feedstocks sheds lights on both basic and applied research for the up-coming establishment of 3G biorefineries.
© 2023 Institute of Process Engineering, Chinese Academy of Sciences. Publishing services by Elsevier B.V. on behalf of KeAi Communications Co., Ltd. This is an open access article under the CC BY-NC-ND license (http://creativecommons.org/licenses/by-nc-nd/4.0/).

1. Introduction

The fast development of global energy consumption has intensified environmental and climatic challenges and increased the demand for use of sustainable feedstocks [1–3]. Biorefineries are now been classified into three generations based on the feedstock used. First-generation (1G) feedstocks consist of grain, vegetable oil, and other food derivatives. With the population expansion and concerns about food scarcity, the 1G feedstocks has been interest in shifting towards second-generation (2G) feedstocks using plant biomass such as grain straw and bagasse [4]. Currently, there is growing interests in applying third-generation (3G) feedstocks such as CO_2 and its derivatives [5]. However, since most autotrophic microorganisms grow slowly while most heterotrophic microbial cell factories lack the ability to consume C1 compounds, it is valuable to adapt microbial cell factories to C1 metabolism such that they can use both 2G and 3G feedstocks.

2G feedstocks such as plant biomass typically comprises 40–50 % cellulose, 20–40 % hemicellulose, and 20–35 % lignin, all of which are integrated in a complex structure [6].

* Corresponding authors.
E-mail addresses: zihe@mail.buct.edu.cn (Z. Liu), twtan@buct.edu.cn (T. Tan).

https://doi.org/10.1016/j.gee.2023.11.004
2468-0257/© 2023 Institute of Process Engineering, Chinese Academy of Sciences. Publishing services by Elsevier B.V. on behalf of KeAi Communications Co., Ltd. This is an open access article under the CC BY-NC-ND license (http://creativecommons.org/licenses/by-nc-nd/4.0/).

Please cite this article as: K. Wang et al., The transition from 2G to 3G-feedstocks enabled efficient production of fuels and chemicals, Green Energy & Environment, https://doi.org/10.1016/j.gee.2023.11.004

After pretreatment and hydrolysis, plant biomass mainly contains glucose, xylose, lignin, and other chemicals like organic acids, phenolic compounds, furfural, and 5-HMF [7–9]. Several microbial cell factories including *Escherichia coli* [10–12], *Yarrowia lipolytica* [13,14], and *Saccharomyces cerevisiae* [15–17], have been developed to transform glucose and xylose into chemicals and fuels. However, xylose conversion is often limited due to the cofactor imbalance and energy shortage. Many strategies have been explored to address this problem, including changing the cofactor preference of critical xylose transformation genes [18,19], looking for non-cofactor dependent approaches [20,21], and using global regulatory systems to enhance strain's fitness on xylose [22,23]. Lately, as formate can be synthesized efficiently from photocatalysis [24,25] and electrocatalysis [26–29], researchers started to explore the possibility of using formate as an energy source [30–32].

With the concept of 3G biorefinery initiated, which intends to utilize 3G feedstocks to produce chemicals and fuels [5], substantial amounts of research has been conducted. Bar-Even [33,34] and Lee's [35] team have achieved growth of *E. coli* using CO_2 and formate as carbon sources, using the reductive glycine (rGly) pathway [36]. Similarly, using the CBB cycle *E. coli* [37] and *Pichia pastoris* [38] realized autotrophic growth with CO_2 as the only carbon source through laboratory directed evolutions. However, the solubility of CO_2 in fermentation media is low, as is the CO_2 concentration inside the cells, resulting in thermodynamic and kinetic challenges for CO_2 fixation. To address this issue, researchers have tried a variety of approaches, including carboxysome expression [39,40], elevating pressure during fermentation [41,42], and so on. Formate on the other hand has a high solubility and we speculate that combined with expression of formate dehydrogenase, formate could be convenient to increase both intracellular supply of both CO_2 and energy, saving the carbon source for bioproduction.

Here, we introduced the use of multi-feedstocks co-feeding to establish a microbial platform and explore yeast for productions of both bulk and value-added chemicals (Fig. 1). Formate was employed to supply both energy and intracellular CO_2 for cell growth and production. Moreover, we suggested that energy from formate could rectify the reductive force imbalance in xylose conversion and speed up the process. As a demonstration we applied this strategy for producing both bulk chemicals ethanol, important platform chemicals FFAs, as well as value-added chemicals longifolene (Fig. 1).

2. Methods

2.1. Strains and reagents

Plasmids and strains utilized in this study can be found in the Supplementary Tables S3–S4. The *E. coli Trans10* used in plasmid constructions was from Quanshijin Biotechnology Co., Ltd. Prime STAR, Prime STAR Max for PCR, and DNA maker were purchased from TaKaRa (Takara Biomedical Technology (Beijing) Co., Ltd.). Restriction enzymes from New England Biolabs (Ipswich, MA, USA) were used in plasmid construction. 2 × Taq PCR mix from Biomed (Beijing, China) was used for colony verifications. The DNA gel purification kits and plasmid extraction kit used in this study were from Omega Biotek (Georgia, USA). Frozen-EZ Yeast transformation II kit II was purchased form ZYMO RESERCH (USA). Codon-optimized heterologous genes were synthesized by Sangon Biotech (Shanghai, China), and oligonucleotides were synthesized by BGI Group (Shenzhen, China). Chemicals were purchased from Sinopharm Chemical (Beijing, China), unless otherwise specified. FAME mixture and longifolene were purchased from Sigma–Aldrich (St. Louis, MO, USA). All chemicals including analytical standards were purchased from Sinopharm Chemical unless stated otherwise.

2.2. Strain cultivation

E. coli strains were grown at 37 °C with constant agitation (200 r min^{-1}) in a medium consisting of 5 g L^{-1} yeast extract (OXOID), 10 g L^{-1} tryptone (OXOID), 10 g L^{-1} NaCl, and when necessary, 80 mg mL^{-1} ampicillin was added to the mixture.

The wildtype strains yeast strain was grown in YPD medium with 2 % glucose. Genetically modified yeast strains were grown on synthetic medium, composed of 1.7 g L^{-1} YNB without amino acids and $(NH_4)_2SO_4$ (Sangon Biotech (Shanghai) Co., Ltd.), 5 g L^{-1} $(NH_4)_2SO_4$, 1.655 g L^{-1} amino acid mixture, and 0.086 g L^{-1} uracil and/or 0.086 g L^{-1} histidine and/or 0.173 g L^{-1} leucine were supplemented when needed. Yeast strains were grown in a temperature-controlled shaker at 30 °C with an agitation speed of 200 r min^{-1}. The specific configuration of reagents could be referred to our previously publications [30,43].

Batch fermentations for the production of free fatty acids and longifolene were performed in a minimal (MM) medium containing 5 g L^{-1} ammonium sulfate, 14.4 g L^{-1} potassium phosphate, 0.5 g L^{-1} magnesium sulfate, 20 g L^{-1} glucose, 30 g L^{-1} xylose, and/or 10 g L^{-1} formate, along with trace metal and vitamin solutions [44]. Additionally, uracil (40 mg L^{-1}), histidine (40 mg L^{-1}), and/or leucine (100 mg L^{-1}) were supplemented when necessary. The minimal medium was modified for ethanol production by adding more $(NH_4)_2SO_4$ (7.5 g L^{-1}) and the anaerobic fermentation process was performed in shaking flasks. The biphasic fermentation was conducted for longifolene production and longfolene is extracted into the organic phase (n-nonane). Inoculation of the cultures was done using 48-h precultures with an initial OD600 of ~5 in 30 mL minimal medium, and the cultures were cultivated for 96 h at 200 r min^{-1} and 30 °C.

2.3. Genetic manipulation

To construct FFAs producing strains, *LEU2* were knockout by Cas9-based genetic modifications [45] in the YJZ08 strain [44]. For ethanol producing strains, *LEU2* and

Please cite this article as: K. Wang et al., The transition from 2G to 3G-feedstocks enabled efficient production of fuels and chemicals, Green Energy & Environment, https://doi.org/10.1016/j.gee.2023.11.004

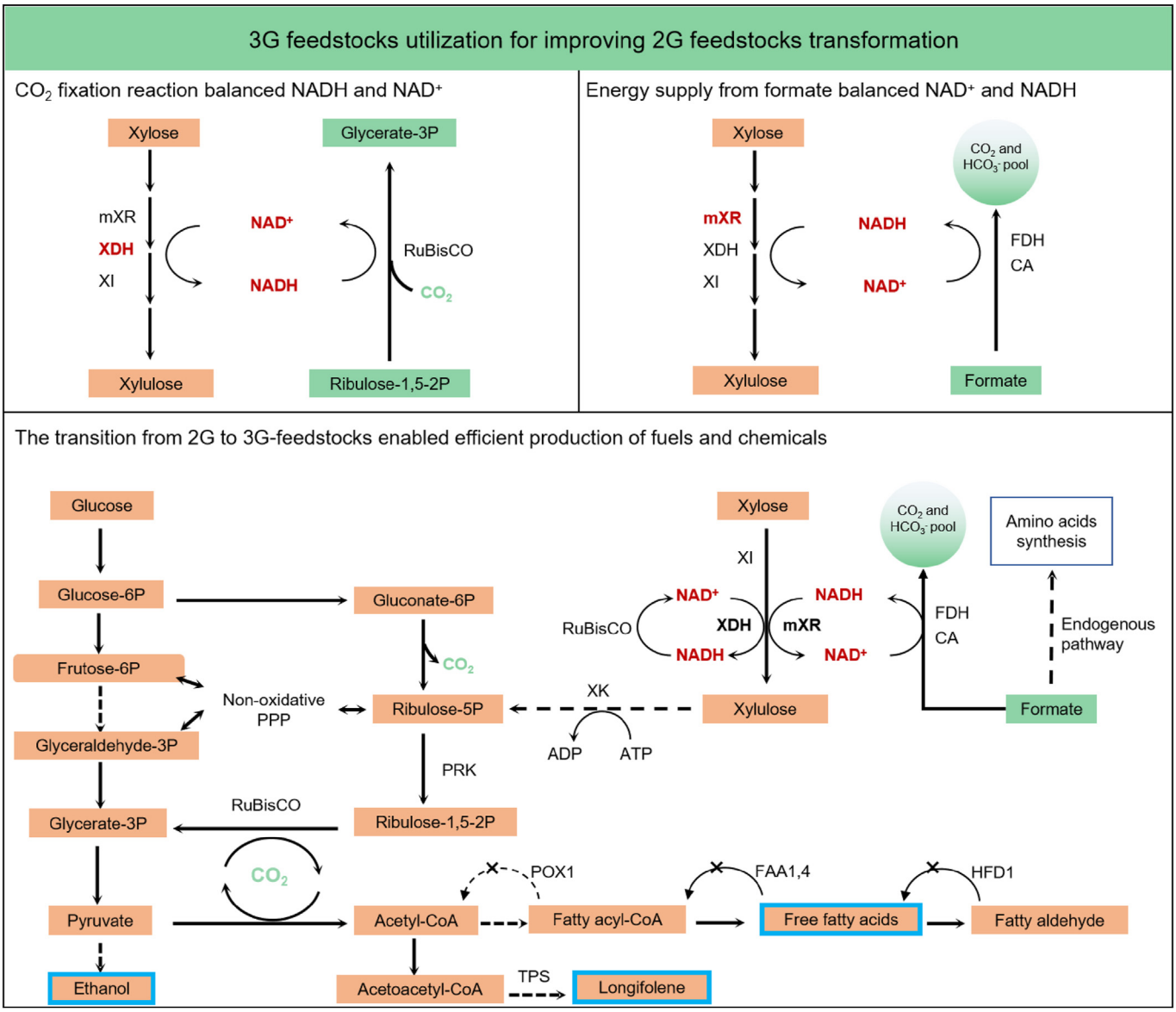

Fig. 1. Schematics diagram of 3G feedstocks utilization for improving 2G feedstocks transformation. The graph illustrates how the reduction imbalance in the xylose conversion process is addressed through the adjustment of the reduction force using formate and formate dehydrogenase (FDH), as well as how the one-carbon utilization efficiency is improved using the CO_2 fixation cycle, the Calvin-Benson-Bassham (CBB) cycle and carbonic anhydrase (*CA*). Additionally, the method was used for de novo synthesis of ethanol, FFAs and longifolene feedstocks. Xylose is assimilated by the oxidoreductive route consisting of *mXR* (mutant of xylose reductase), *XDH* (xylitol dehydrogenase), *XK* (xylulose kinase), and *XI* (xylose isomerase). For FFAs production, fatty acyl-CoA synthetase encoding genes *FAA1* and *FAA4*, fatty acyl-CoA oxidase encoding gene *POX1* and fatty aldehyde dehydrogenase *HFD1* were knockout. For longifolene production, the longifolene synthase gene *TPS* was expressed.

HIS3 were knockout by the same method in the *S. cerevisiae* CEN.PK 113-5D. Primers are listed in the Supplementary Table S5.

Gene sequences of formate dehydrogenase (FDH) from various hosts were sourced from the National Center for Biotechnology Information (NCBI) website (https://www.ncbi.nlm.nih.gov/). Plasmids were constructed using PCR, gel recovery, enzyme digestion, or homologous recombination. All gene constructs were confirmed by sequencing. All codon optimized heterologous genes are listed in the Supplementary Table S6.

2.4. Quantitative analysis

Biomass was determined by measuring optical density at 600 nm (OD_{600}) using an EU-2600 Visible Spectrophotometer (Shanghai Onlab instrument, China).

The measurement of extracellular metabolites, including glucose, xylose, formate, and ethanol, was performed using a Shimadzu LC-20AT HPLC system (Japan) with both RID and UV detectors at 210 nm. The analysis was conducted with a flow rate of 0.6 mL min^{-1}, using 5 mM H_2SO_4 as the eluent and Aminex HPX-87H column (Bio-Rad) at 65 °C. A 10 μL

Please cite this article as: K. Wang et al., The transition from 2G to 3G-feedstocks enabled efficient production of fuels and chemicals, Green Energy & Environment, https://doi.org/10.1016/j.gee.2023.11.004

sample was injected, and HPLC standards were created by diluting a mixture of 10 g L^{-1} glucose, 10 g L^{-1}xylose, 10 g L^{-1} formate, and 10 g L^{-1} ethanol into 6 different gradient concentrations using the eluent.

Samples for FFAs were measured using gas chromatography–mass spectrometry after derivatization, as stated in our recent paper [46,47].

Samples for longifolene detection were taken from the upper organic phase and analyzed using gas chromatography–mass spectrometry (Agilent Technology INC.), as previously described in our publication [43].

2.5. Transcriptomics analysis

For the transcriptomics analysis, both KW201 and KW802 were grown in minimal medium containing 20 g L^{-1} glucose, 30 g L^{-1} xylose, and 10 g L^{-1} formate at 30 °C, 200 r min^{-1} for 96 h. Samples were collected at specific intervals based on the progression of the experiment (Prophase-24 h, metaphase-48 h, anaphase-72 h, final-96 h). Transcriptomic detection was completed by Novgene Biotech Co., Ltd. NovoMagic platform of Novgene Biotech Co., Ltd.

2.6. ^{13}C metabolic analysis and the NADH/NAD^+ test

To demonstrate the C1 efficiency and the contribution of each carbon source in the engineered strains, strains were fermented in MM with 20 g L^{-1} $^{13}C_6$-glucose, 30 g L^{-1} xylose, 10 g L^{-1} formate; 20 g L^{-1} glucose, 30 g L^{-1} $^{13}C_5$-xylose, 10 g L^{-1} formate; 20 g L^{-1} glucose, 30 g L^{-1} xylose, 10 g L^{-1} ^{13}C-formate, respectively. The labelling profiles of center metabolites and amino acids were examined after 96 h using liquid chromatography-mass spectrometry (LC-MS, ThermoFisher) [48].

The efficiency of C1 assimilation was derived from the outcomes of the ^{13}C metabolic analysis (Fig. 2i and j). utilising the procedure delineated in prior research[26]. In particular, we totalled each constituent within the entire gamut of examined metabolites, using 100 % as the benchmark or denominator. Subsequently, we compiled the percentage contribution of ^{13}C from each constituent within all assayed metabolites to establish the numerator. The C1 assimilation efficiency was then calculated by contrasting these two figures.

The NADH/NAD^+ ratio of each sample was performed using the WST-8 NADH/NAD^+ test kit (Beyotime Biotechnology) as the manufacturer's instructions.

2.7. Preparation of cellulose hydrolysates

Corn stover was pretreated by steam explosion (SE) at COFCO Biochemical Energy (Zhaodong) Co., Ltd. The operating condition of the 15 L pilot steam explosion reactor was maintained at 170 °C for 5 min, followed by a sudden release of pressure to atmospheric pressure. Corn stover (43.8 ± 2.8 % glucan, 18.6 ± 2.2 % xylan, 28.3 ± 2.6 % lignin) was soaked in 2 % (w w^{-1}) dilute sulfuric acid solution for 1.5h at 50 % solid loading before steam explosion treatment. Cellulase (Cellic Ctec2) was obtained from Novozymes with enzyme activity of 120 ± 10 FPU ml^{-1}. The operating conditions for enzymatic hydrolysis have been mentioned in the previous work [49]. The detoxification step was performed to partially remove inhibitors from the SE pulp hydrolysates. As previously described, the hydrolysate was passed through a glass column packed with activated carbon and the effluent was collected at the end of the column [50,51].

3. Results and discussion

3.1. Formate enables efficient FFA production on xylose

There are two metabolic routes for converting xylose through the pentose phosphate pathway. The first route involves reduction and dehydrogenation (RD route), that may result in an imbalance of the intracellular reductive force, limiting the conversion of xylose [20]. The second route utilizes xylose isomerase (XI) to convert xylose that does not result in the production or consumption of reducing power. However, the enzyme activity is low, impacting the conversion of xylose [52]. Furthermore, to evaluate the impact of this method on FFAs production, the FFAs-producing strain YJZ08 was selected as the host strain for FFAs production. Thus, we started by evaluating these two pathways for xylose utilization. The RD route exhibited a high xylose conversion rate of 0.39 g L^{-1} h^{-1} (KWT101) in the cultures with 20 g L^{-1} glucose and 30 g L^{-1} xylose, while the xylose conversion rate of the XI route was as low as 0.03 g L^{-1} h^{-1} (KWT102). We then combined the two xylose utilization routes (KWT103) and improved the xylose conversion rate to 0.43 g L^{-1} h^{-1} (Fig. 2a).

To rectify the reductive force imbalance in xylose conversion, formate dehydrogenase (*FDH*) from various species were expressed in strains KWT103 and KWT201 (an ethanol-producing strain genetically modified from CEN.PK 113-5D), so that formate could be transformed into CO_2 and generate the reducing power. Interestingly, we found that the introduction of *FDHs* could significantly boost the xylose conversion rate (Fig. 2b). The co-consumption of 20 g L^{-1} of glucose, 30 g L^{-1} of xylose and 10 g L^{-1} of formate resulted in 44 % (KWT306, 0.62 g L^{-1} h^{-1}) and 42 % (KWT406, 0.61 g L^{-1} h^{-1}) improvements in conversion rate of xylose under aerobic or micro-aerobic conditions, respectively. The consumption rate of formate reached 0.04 g L^{-1} h^{-1} and 0.05 g L^{-1} h^{-1}, respectively, which were 160 % and 229 % compared with their control group (Fig. 2b and c). Meanwhile, we discovered that xylose was completely consumed by strain KWT201 under aerobic conditions, whereas in the micro-aerobic conditions there was more xylose residues that might be caused by insufficient ATP or NAD(P)H supply [23,53]. Furthermore, we explored the possibility whether the introduction of *FDHs* could achieve simultaneous conversion of glucose and xylose. Yet the strain's glucose intake was only moderate accompanied with xylose consumption. Basically, only ~4 g L^{-1} xylose was consumed together with glucose within 10 h, and the majority of xylose was

Please cite this article as: K. Wang et al., The transition from 2G to 3G-feedstocks enabled efficient production of fuels and chemicals, Green Energy & Environment, https://doi.org/10.1016/j.gee.2023.11.004

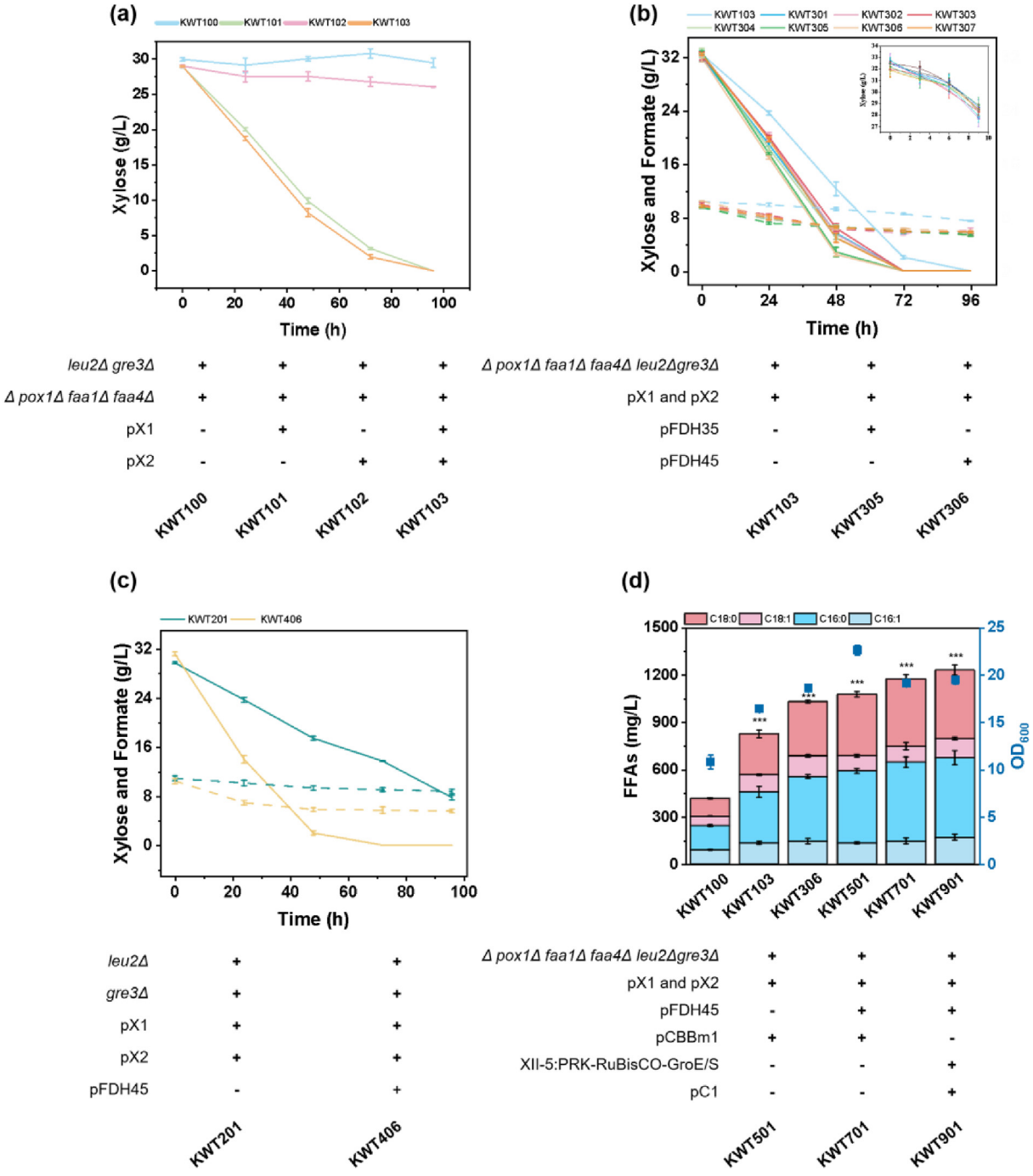

Fig. 2. The utilization of formate improved utilizations of 2G feedstocks for FFAs production. (a) Xylose consumption obtained with the xylose transformation strains feeding with 20 g L^{-1} glucose and 30 g L^{-1} xylose. (b) Xylose (solid line) and formate (dotted line) consumption obtained with the xylose and formate transformation strains under aerobic conditions feeding with 20 g L^{-1} glucose, 30 g L^{-1} xylose and 10 g L^{-1} formate. The inner illustration shows the xylose consumption of the strain for 0–9 h. (c) Xylose (solid line) and formate (dotted line) consumption obtained with the xylose and formate transformation strains under micro aerobic feeding with 20 g L^{-1} glucose, 30 g L^{-1} xylose and 10 g L^{-1} formate. (d) FFAs production and growth. All data represents the mean ± s.d., and error bars indicate standard error (n = 3).

consumed after glucose was depleted (Fig. 2b, Supplementary Fig. 2).

Meanwhile, the strain KWT103 was able to produce FFAs at a titer (826 mg L^{-1}), which was about 2-fold higher than that of KWT101 (416 mg L^{-1}). Furthermore, the strain KWT306 was obtained by expressing the formate conversion module in the strain KWT103, that exhibited enhanced FFAs production reaching 1030 mg L^{-1}, which was 25 % higher than that of the KWT103 strain (Fig. 2d).

3.2. *Engineering* S. cerevisiae *for* CO_2 *utilization*

During the conversion process of 2G feedstocks, a substantial amount of carbon is released as CO_2, leading to a low

Please cite this article as: K. Wang et al., The transition from 2G to 3G-feedstocks enabled efficient production of fuels and chemicals, Green Energy & Environment, https://doi.org/10.1016/j.gee.2023.11.004

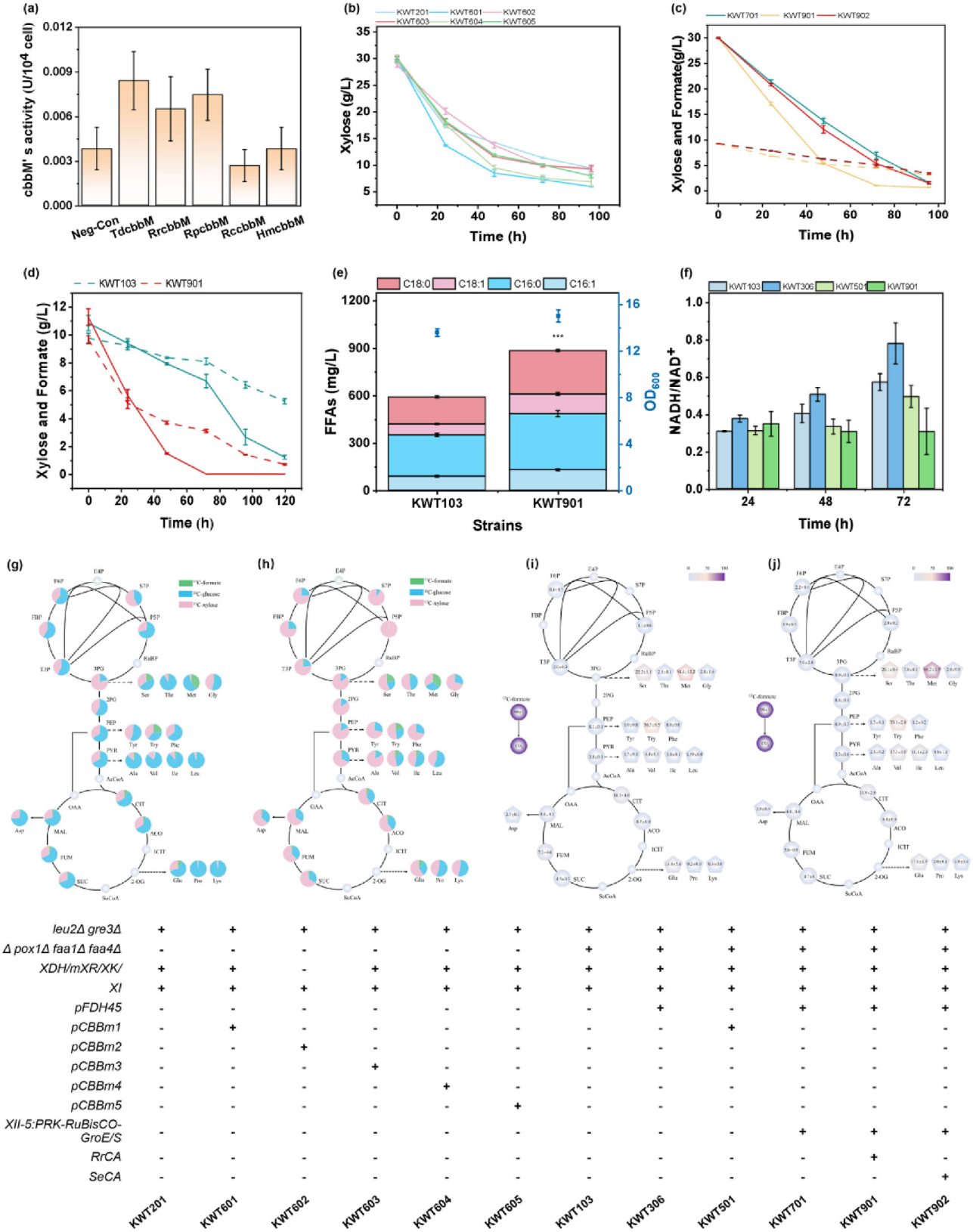

Fig. 3. The construction and application of carbon-fixing strains, along with metabolomic analysis, demonstrated the high xylose utilization and formate assimilation capacity of strain KWT901. (a) The The cbbM's activity from different species; (b) Xylose consumption of the strains expressing different cbbM genes in shake flasks feeding with 20 g L^{-1} glucose and 30 g L^{-1} xylose; (c) Xylose (solid line) and formate (dotted line) consumption in engineered strains for CA enzyme screening in shake flasks feeding with 20 g L^{-1} glucose, 30 g L^{-1} xylose and 10 g L^{-1} formate; (d) Xylose (solid line) and formate (dotted line) consumption of engineered strains in non-detoxified cellulose hydrolysate with 10 g L^{-1} formate; (e) FFAs production of engineered strains in non-detoxified cellulose hydrolysate with 10 g L^{-1} formate; (f) NADH/NAD $^{+}$ test of representative strains at different time points. ^{13}C labeling experiments indicated the carbon

Please cite this article as: K. Wang et al., The transition from 2G to 3G-feedstocks enabled efficient production of fuels and chemicals, Green Energy & Environment, https://doi.org/10.1016/j.gee.2023.11.004

carbon yield [54]. To enhance C1 assimilation efficiency and effectively integrate 2G and 3G biorefinery, it is necessary to address this issue. Therefore, after successfully implementing the formate conversion module, key enzymes of the CBB cycle including *PRK*, *cbbM*, and chaperone *GroE/S* (CBB module, CBBm) were introduced into the strain to facilitate CO_2 fixation and improve carbon conversion efficiency [55]. Specially, *cbbM* genes from different species were tested in the KWT201, and the *cbbM* gene from *Thiobacillus denitrificans* exhibited efficient enzyme activity and xylose consumption in *S. cerevisiae* (Fig. 3a and b). The screened CBBm was then integrated into the FFAs production and xylose conversion strain KWT103 yielding strain KWT501. This resulted in an improved xylose conversion rate by 32.6 % (0.57 g L^{-1} h^{-1}) (Supplementary Fig. 3). This improvement can be attributed to the introduction of CBBm, which to some extent alleviated the cofactor imbalance issue associated with xylose conversion [55]. Moreover, the copy number of CBBm was increased yielding strain KWT502, however, a high copy number of CBBm seemed to reduce the xylose conversion rate to 0.48 g L^{-1} h^{-1}, with xylose residuals remained in the late fermentation stage (Supplementary Fig. 3).

We then speculated whether this result was because of low intracellular CO_2 concentrations. The solubility of CO_2 is low, and the gas–liquid mass transfer efficiency of CO_2 might be insufficient. Thus, carbonic anhydrase (CA) that facilitates CO_2 hydration into H_2CO_3, H^+, HCO_3^-, and promotes the transmembrane transport of CO_2. This approach can enhance the concentration of CO_2 in the cell, especially in close proximity to the RubisCO enzyme [56,57], thus improving the thermodynamic and kinetics of the reaction. CA from *Rhodospirillum rubrum* and *Synechococcus elongatus* were tested, and the strain of KWT901 expressed the CA from *R. rubrum* showed the best activity according to the higher xylose and formate conversion rate (Fig. 3c). Indeed, compared with KWT701, the xylose conversion rate of the KWT901 strain increased by 51.0 %. Moreover, these strains exhibited enhanced FFAs production reaching 1076 mg L^{-1} (KWT501), 1173 mg L^{-1} (KWT701) and 1230 (KWT901) mg L^{-1}, which was 1.30, 1.42, and 1.49 times higher than with the KWT306 strain (Fig. 2d).

Furthermore, the engineered yeast KWT103 and KWT901 were verified in 2G raw material-cellulose hydrolysate. Main components of SE hydrolysate before and after detoxification can be found in Supplementary Table 1. The strain KWT901 had excellent phenotype in both detoxified and non-detoxified hydrolysates (Supplementary Fig. 4), and the xylose conversion rate reached 0.09 g L^{-1} h^{-1} in the hydrolysates without detoxification steps, with all xylose consumed within 120 h (Fig. 3d). Similarly, the strain KWT901 had better formate consumption and FFAs production, achieving rates of 0.09 g L^{-1} h^{-1} and 842 mg L^{-1}, respectively (Fig. 3d and e).

To analyze central carbon metabolisms of the engineered strains for co-utilizing 2G and 3G feedstocks, we perform ^{13}C labeled analysis on strains KWT103 and KWT901 with labeled glucose, xylose and formate, respectively. The xylose-labeled experiment indicated that compared with that of KWT103 the ^{13}C fraction of center carbon metabolite and amino acids in KWT901 increased significantly. Specially, the ^{13}C labeled center carbon metabolites and amino acids in the KWT103 were primarily derived from glucose (Fig. 3g), whereas those of KWT901 were primarily derived from xylose (Fig. 3h), indicating that the xylose metabolism of KWT901 was substantially improved. Detailed results of the labeling experiment are provided in Supplementary Fig. 5a and b and 5c-d.

In the process of performing labeling experiments with ^{13}C-formate, it came as a surprise that ^{13}C-labeled amino acids were plentiful in both KWT103 and KWT901. Even for KWT103 lacking the formate conversion module and CO_2 fixation module, citrate together with four amino acids, including glutamate, serine, tryptophan, and methionine, were labelled in the more than 10 % (Fig. 3i). We thus speculated that *S. cerevisiae* has an endogenous formate utilizing pathway possibly based on amino acid rearrangements, that converts formate into glutamate, serine, tryptophan, and methionine. Hence, we discovered that *S. cerevisiae* exhibited a strong assimilation capacity for formate. The primary route for its integration into the metabolic flux was through the conversion of the rGly pathway metabolite, a 5,10-methylenetetrahydrofolate. Consequently, consideration should be given to key enzymes in this pathway, such as *MIS1*, *MTD1*, and *ECM31* in future research. The strain KWT901 also exhibited effective CO_2 fixation as stated by the ^{13}C-labelling analysis. When cultured with 20 g L^{-1} glucose, 30 g L^{-1} xylose and 10 g L^{-1} ^{13}C-labeled formate as feedstocks, the ^{13}C labelling methionine in KWT901 achieved a 66.2 % enrichment. Moreover, compared with the KWT103 strain, the m+2 isotopomer proportion exhibited a 65.43 % increase, achieving a labeling rate of 9.0 %. The KWT901 strain showed the greatest ^{13}C labeling rate enhancement for valine at 17.3 %, which was 3.93 times higher than the control group's rate of 4.4 % (Fig. 3j). This enhancement may be attributed to the metabolic rearrangement of methionine. Moreover, 3-phosphoglycerate was labeled in KWT901 but not in KWT103, confirming that the CO_2 produced from formate could be fixed via the CO_2 fixation pathway. After testing and analyzing the detected ^{13}C-metabolites, we discovered that wild type brewing yeast

contribution of formate, glucose, and xylose in strain (g) KWT103 and (h)KWT901.^{13}C labeling experiments indicated the carbon contribution of formate in strain (i) KWT103 and (j) KWT901. Abbreviations: F6P, fructose 6-phosphate; FBP, fructose-1,6-diphosphate; T3P, triose-3-phosphate; 3 PG, 3-phosphoglycerate; RuBP, ribulose bisphosphate; P5P, pentose-5-phosphate; S7P, sedoheptulose 7-phosphate; E4P, erythrose 4-phosphate; 2 PG, 2-phosphoglycerate; PEP, phosphoenolpyruvate; PYR, pyruvate; AcCoA, acetyl-CoA; CIT, citrate; ACO, cis-aconitate; ICIT, iso-citrate; 2-OG, 2-oxoglutarate; SuCoA, succinyl-CoA; SUC, succinate; FUM, fumarate; MAL, malate; OAA, oxaloacetate; Ser, serine; Thr, threonine; Met, methionine; Gly, glycine; Tyr, tyrosine; Try, tryptophan; Phe, phenylalanine; Ala, alanine; Val, valine; Ile, isoleucine; Leu, leucine; Asp, Aspartic acid; Glu, glutamic acid; Pro, proline; Lys, lysine. All data represent the mean ± s.d. , error bars indicate standard error (n = 3).

Please cite this article as: K. Wang et al., The transition from 2G to 3G-feedstocks enabled efficient production of fuels and chemicals, Green Energy & Environment, https://doi.org/10.1016/j.gee.2023.11.004

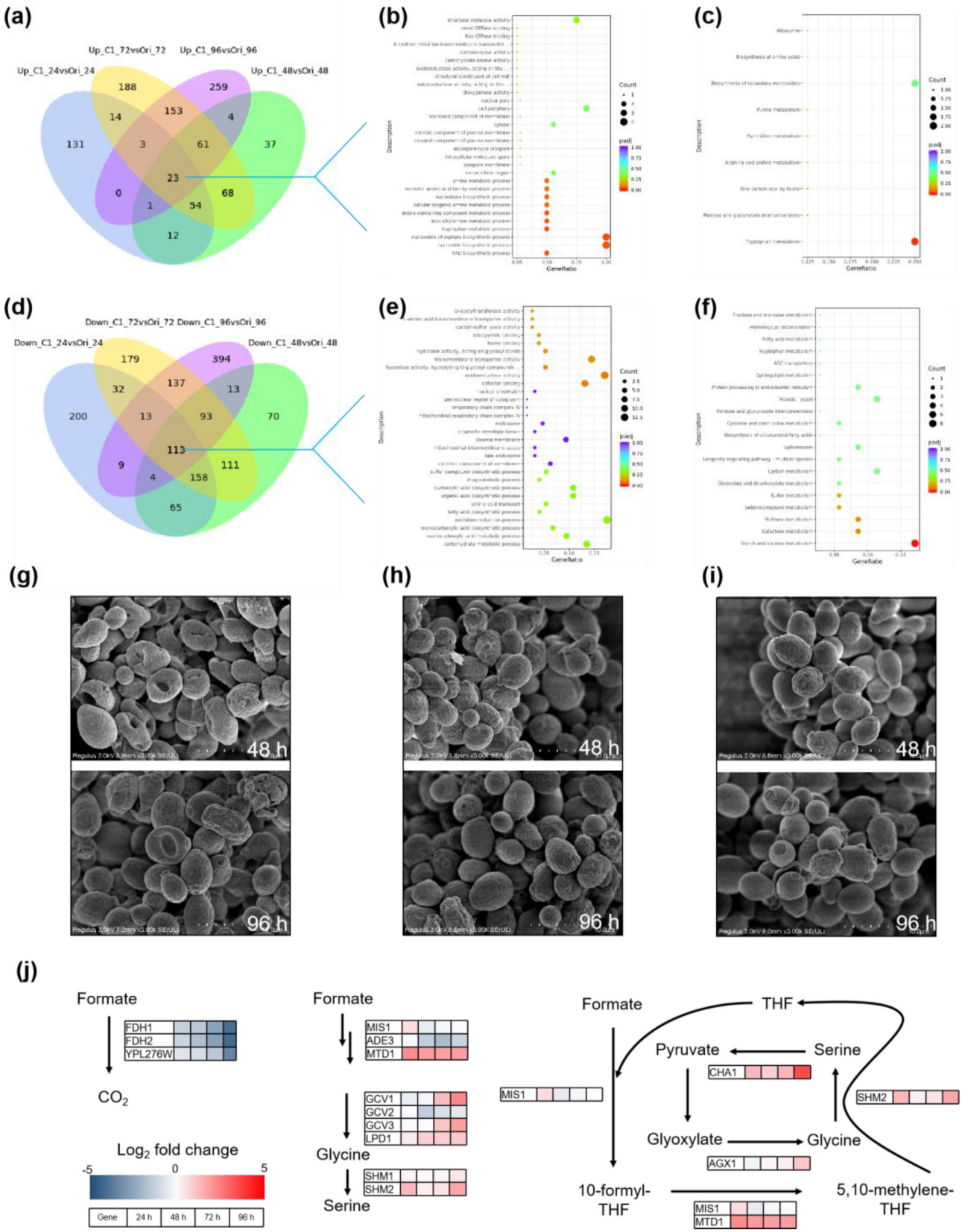

Fig. 4. Transcriptomic and cell morphology analysis for strains with formate addition. (a) 23 commonly up-regulated genes (adjusted P value < 0.05, Benjamini–Hochberg method, and absolute value of log2 FC > 1) were identified comparing KWT802 with KWT201 at different stages of fermentation (24, 48, 72 and 96 h). (b) GO slim categories for the 23 common up-regulated genes. (c) The KEGG terms analysis for the 23 common up-regulated genes. (d) 113 commonly down-regulated genes (adjusted P value < 0.05, Benjamini–Hochberg method, and absolute value of log2 FC > 1) were identified comparing KWT802 with KWT201 at different stages of fermentation (24, 48, 72 and 96 h). (e) GO slim categories for the 113 common down-regulated genes. (f) The KEGG terms analysis for the 113

Please cite this article as: K. Wang et al., The transition from 2G to 3G-feedstocks enabled efficient production of fuels and chemicals, Green Energy & Environment, https://doi.org/10.1016/j.gee.2023.11.004

exhibits good C1 assimilation efficiency. Specifically, when used in conjunction with glucose and xylose, about 6.3 % of the cellular carbon originates from formate. After enhancing the process through one-carbon metabolism modification, we were able to further increase this to 9.2 % (Supplementary Table 2). The detailed results of the ^{13}C-formate labeled experiment can be found in Supplementary Fig. 6.

Citrate was also labelled strongly, with ^{13}C-labelling rates of 14.6 % and 11.9 % in KWT103 and KWT901, respectively (Fig. 3i–j). This might be because the carboxylation catalyzed by pyruvate carboxylase also plays an important role in the carbon fixation in *S. cerevisiae* [58]. All measured pyruvate-derived and 2-oxoglutarate-derived amino acids gained more ^{13}C-labeling in the KWT901, e.g. alanine, valine, isoleucine, leucine, glutamate, proline, lysine, with the ^{13}C-labelling rate of glutamate, valine and isoleucine exceeding 10 %, indicating the enriched energy supply and intracellular CO_2 concentration further benefit carbon fixation through amino acid metabolism. This hypothesis has then been supported by redox analysis, that the NADH/NAD$^+$ ratio of strains supplied with the FDH module retained a high level throughout the fermentation stage. The highest NADH/NAD$^+$ ratio appeared to be 0.78 in KWT306 at 72h (Fig. 3f), that is 37 % higher than the control group. It was important to note that the xylose reductase (XR) employed in our study was the mutated mXR^{R276H} variant, which exhibited a higher preference for NADH as a cofactor [55]. The results that the NADH producing FDH improves xylose utilization maybe a combinational effect of the improved reductive force balance together with the energy provision. Moreover, the NADH/NAD$^+$ ratio also showed that when CBBm was expressed, the intracellular reducing power was consumed resulting in reduced NADH/NAD$^+$ ratio (0.49). The NADH/NAD$^+$ ratio was further reduced to 0.31, when CA is overexpressed. Considering that the extra energy supplement was derived from formate, these results confirmed that co-utilization of formate together with glucose and xylose facilitated an ample supply of energy in *S. cerevisiae*, that could contribute to enhanced xylose consumption and may even to bioproduction of energy-intense chemicals.

3.3. Transcriptome analysis revealed global metabolic re-arrangements

To investigate how one-carbon metabolism engineering enhances xylose conversion and carbon conservation, we carried out transcriptome analysis on the strains KWT201 and KWT802. Differentially expressed genes at various fermentation stages (24, 48, 72, and 96 h) were used for analysis. The number of differentially expressed genes showed an increasing trend with the extension of fermentation time (Supplementary Fig. 7). According to the gene ontology (GO) and KEGG analysis, significantly regulated genes between the two strains enriched in the redox process, transmembrane transportation, carbon metabolism and secondary metabolism (Supplementary Fig. 8a–h).

Further analysis of gene expressions at different stages identified 23 genes that were upregulated and 113 genes that were downregulated throughout the fermentation. GO and KEGG pathway analysis on these genes revealed that nucleotide biosynthesis and tryptophan metabolism were enriched and upregulated (Fig. 4a–c), whereas oxidoreductase activity, as well as starch and sucrose metabolism were enriched and downregulated (Fig. 4d–f). Additionally, analysis revealed that the top 10 transcription factors (TFs) that bind to the 113 down-regulated genes all involved in stress response, as well as the control of carbon source quality and availability (Supplementary Fig. 9). No associated TFs were identified among the 23 up-regulated genes.

Additionally, when 10 g L^{-1} of formate was introduced at the start of fermentation we observed significant changes in the cell morphology of strain KWT201 during the middle and late fermentation stages (Fig. 4g). This included cell collapse and roughening of most cell surfaces. In the absence of formate, the strain displayed typical growth, development, and cell death characteristics. Moreover, when 10 g L^{-1} of formate was added during the fermentation of engineered strain KWT802, which contained the one-carbon conversion module, the cells remained relatively normal in comparison to the control group (Fig. 4g–i). These results indicated that the one-carbon conversion module could alleviate the toxic effects of formate, highlighting the benefits of this strategy in formate conversion.

Taking together, we noticed that compared with that of KWT201 most genes related to the EMP and TCA pathways have been up-regulated in KWT802, whereas genes in the oxidative PP pathway, such as *ZWF1*, *GND1* and *GND2*, had been down-regulated, indicating that the regulation of intracellular redox levels plays a key role in xylose conversion (Supplementary Fig. 10). Interestingly, most genes in the rGly and gSerine pathway [59] (Formate conversion to serine pathway) were significantly up-regulated, which may be associated with the prominent ^{13}C-formate labeling observed in serine (Fig. 4j). This result was consistent with the KEGG pathway analysis, that pathways regarding amino acid metabolism remained significantly regulated throughout the whole fermentation (Supplementary Fig. 8e–h). Analysis regarding the amino acid biosynthesis and degradation processes also indicated that genes involved in the tryptophan and glutamate synthetic pathways were significantly upregulated, such as:

common down-regulated genes. (g) Cell morphology of KWT201 strain at 48h and 96 h cultured in with the addition of 10 g L^{-1} formate. (h) Cell morphology of KWT802 strain at 48/96 h without the addition of formate. (i) Cell morphology of KWT802 strain at 48h and 96 h with the addition of 10 g L^{-1} formate (j) Transcriptional regulations involved in the formate metabolism (From left to right, formate oxidation pathway, rGly pathway and gSerine pathway [59]). Transcriptomic analysis was performed by Novgene Biotech Co., Ltd. NovoMagic platform (https://magic.novogene.com/customer/main#/loginNew). Strains were cultivated in the MM medium with 20 g L^{-1} glucose, 30 g L^{-1} xylose and 10 g L^{-1} formate in biological triplicates. Samples were taken at 24h, 48h, 72h and 96h. All strains were cultivated in biologically triplicates.

Please cite this article as: K. Wang et al., The transition from 2G to 3G-feedstocks enabled efficient production of fuels and chemicals, Green Energy & Environment, https://doi.org/10.1016/j.gee.2023.11.004

ARO1-4, *TRP3-5* and *GDH3*, which was consistent with the corresponding ^{13}C-formate labeling experiment (Fig. 3i–j and Supplementary Fig. 11). These findings suggested that endogenous formate utilization pathways (primarily coupled with THF conversion) and CO_2 fixation pathways may play a role in the global regulatory mechanisms of the synthesis and degradation of these amino acids. We hypothesized that CO_2 and formate utilization in *S. cerevisiae* may hold potentials for the synthesis of these amino acids.

3.4. Enhanced ethanol and longifolene production via co-utilization of 2G and 3G feedstocks

After demonstrating the efficient xylose consumption and energy balance through co-utilization of 2G and 3G feedstocks, we investigated the effectiveness of this strategy for production of ethanol and longifolene. Ethanol is an essential bulk chemical that can be used to make drinks, essences, fuels, and other products. However, ethanol production results in production of CO_2, e.g. one mole of CO_2 per mole of ethanol formed. The co-utilization of 2G and 3G feedstocks provides opportunities to re-capture emitted CO_2, while using formate as energy transmitter to provide energy from renewable sources. Similar with the results of FFAs production, the ethanol production of engineering strains KWT406, KWT601, KWT801 and KWT802 increased by 6.83 %, 15.05 %, 9.21 %, and 18.40 %, respectively, compared with that of the control group (KWT201). Notably, KWT802 displayed the highest ethanol production, reaching 15.21 g L^{-1} (Fig. 5a).

Meanwhile, we also tested our strategy for productions of value-added chemicals. Longifolene can be used as an ingredient in the production of synthetic resin, synthetic scent, and flotation agents. Also, it has a high energy density and a high combustion heat, making it an ideal alternative for aviation kerosene [43,60,61]. Similar with the above production strains, each module was integrated into the longifolene production strain containing longifolene synthesis gene *TPS* obtaining strains KWT101-105, respectively. The final strain KWT105 exhibited a production of longifolene reaching 1.50 mg L^{-1}, which is ~2-fold of KWL101 with only the xylose conversion module (Fig. 5b).

3.5. Discussion

In this study, to address the issue of cofactor imbalance in xylose conversion during the conversion of 2G substrates, a method using 3G substrates had been proposed. During the construction of the xylose metabolic pathway, we employed a mutated version of xylose reductase, referred to as mXR^{R276H}, which exhibits a higher preference for NADH. Moreover, the consideration of an NADP$^+$-dependent FDH was also an intriguing alternative. Normally, xylose reductase favors NADP$^+$, and an imbalance in NADPH/NADP$^+$ could result in a bottleneck for xylose utilization. Thus, by incorporating an NADP$^+$-dependent FDH, the cofactor ratios also can be adjusted to support more efficient xylose uptake and conversion. This can further expand the application of 3G substrates, and even further by combining and regulating the expression of both NAD$^+$- and NADP$^+$-dependent FDHs, thereby further enhancing the efficiency of xylose conversion under different conditions.

Moving into the 3G biorefinery, several key challenges and opportunities should be considered, including the choice of the C1 compound (CO_2, formate, methanol, methane etc.), and the tuning of sugar metabolism of microbial cell factories to C1 metabolism. In this work, we reported the efficient co-consumption of 2G and 3G feedstocks as a biorefinery strategy to improve the carbon fixation and energy utilization in *S. cerevisiae* for productions of bulk-, platform-, and value-added chemicals. We reported that wildtype *S. cerevisiae* exhibited a decent C1 assimilation efficiency, i.e. when co-utilization with glucose and xylose, ~6.3 % of the cellular carbon was derived from formate, while we managed to enhance it further to 9.2 %. The success in improving carbon fixation efficiency and the realization of value-

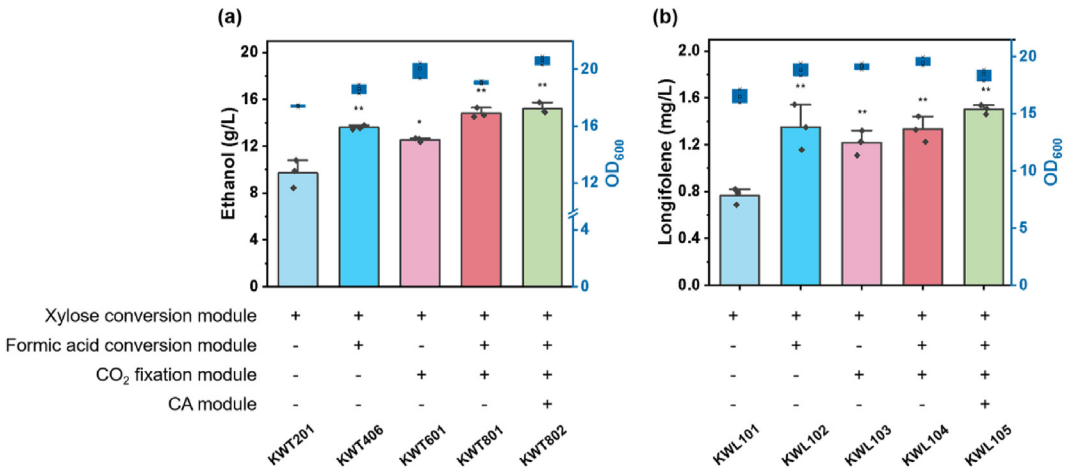

Fig. 5. Demonstration of the co-utilization strategy for productions of bulk-chemicals ethanol and value-add chemicals longifolene. (a) Ethanol production. (b) Longifolene production. A two-tailed Welch's t-test was used to assess the statistical significance between groups (*P < 0.05; **P < 0.01; ***P < 0.001). All data represents the mean ± s.d., and error bars indicate standard error of biological triplicates.

Please cite this article as: K. Wang et al., The transition from 2G to 3G-feedstocks enabled efficient production of fuels and chemicals, Green Energy & Environment, https://doi.org/10.1016/j.gee.2023.11.004

added chemical production establishes a strong foundation for future studies in optimizing 3G feedstocks.

Our current research laid the groundwork for such future advancements by demonstrating the feasibility of integrating formate—a 3G feedstock—into the metabolic pathways of *S. cerevisiae*, optimizing the co-consumption of formate with traditional sugars. The carbon from formate was incorporated into the biomass and metabolites, exemplifying an initial step towards a more comprehensive utilization of carbon emissions.

The sustainability of biorefineries was an evolving journey, one where emerging technology play a pivotal role. As our study advanced the co-utilization of 2G and 3G feedstocks in *S. cerevisiae*, it paved the way for considering additional processes that enhanced the overall carbon economy. Technologies such as electrocatalysis or photocatalysis, while not a direct part of this research, represented intriguing future adjuncts that could augment the carbon cycle within biorefinery systems.

In conclusion, our research underpins the potential of a biorefinery ecosystem that harnesses both biological and technological methods for carbon conversion. The prospect of combining microbial bioconversion with technologies like electrocatalysis, photocatalysis, or algal bioprocessing opened exciting avenues for the circular transformation of carbon sources, making the dream of a zero-waste biorefinery increasingly attainable.

Author contributions

K.W., Z.L, J.N. and T.T. designed research; K.W. performed research; C.S., C.Z. and D.C. prepared the cellulose hydrolysate. K.W., H.B., Y.L., M,W., B,C. and Z.L analyzed data; and K.W., Z.L, J.N. and T.T. wrote the paper. All authors read and approved the paper.

Conflict of interest

The authors declare that they have no known competing financial interests or personal relationships that could have appeared to influence the work reported in this paper.

Acknowledgments

This work was supported by the National Key R&D Program of China [2021YFC2103500], National Natural Science Foundation of China (22211530047), Tianjin Synthetic Biotechnology Innovation Capacity Improvement Project [grant numbers: TSBICIP-KJGG-009], the Beijing Advanced Innovation Center for Soft Matter Science and Engineering, Beijing University of Chemical Technology.

Appendix A. Supplementary data

Supplementary data to this article can be found online at https://doi.org/10.1016/j.gee.2023.11.004.

References

[1] W. Qiao, S. Xu, Z. Liu, X. Fu, H. Zhao, S. Shi, Bioresour. Technol. 364 (2022) 128095.
[2] G. Hu, Z. Li, D. Ma, C. Ye, L. Zhang, C. Gao, L. Liu, X. Chen, Nat. Catal. 4 (2021) 395–406.
[3] C.D. Scown, Trends Biotechnol. 40 (2022) 1415–1424.
[4] P. Havlík, U.A. Schneider, E. Schmid, H. Böttcher, S. Fritz, R. Skalský, K. Aoki, S.D. Cara, G. Kindermann, F. Kraxner, S. Leduc, I. Mccallum, A. Mosnier, T. Sauer, M. Obersteiner, Energy Pol. 39 (2011) 5690–5702.
[5] Z. Liu, K. Wang, Y. Chen, T. Tan, J. Nielsen, Nat. Catal. 3 (2020) 274–288.
[6] J.C. Liao, L. Mi, S. Pontrelli, S. Luo, Nat. Rev. Microbiol. 14 (2016) 288–304.
[7] Z. Liu, H. Li, X. Gao, X. Guo, S. Wang, Y. Fang, G. Song, Nat. Commun. 13 (2022) 4716.
[8] D. Cai, P. Li, Z. Luo, P. Qin, C. Chen, Y. Wang, Z. Wang, T. Tan, Bioresour. Technol. 211 (2016) 117–124.
[9] W. Deng, Y. Feng, J. Fu, H. Guo, Y. Guo, B. Han, Z. Jiang, L. Kong, C. Li, H. Liu, P.T.T. Nguyen, P. Ren, F. Wang, S. Wang, Y. Wang, Y. Wang, S.S. Wong, K. Yan, N. Yan, X. Yang, Y. Zhang, Z. Zhang, X. Zeng, H. Zhou, Green Energy Environ. 8 (2023) 10–114.
[10] M. Wei, G. Li, H. Xie, W. Yang, H. Xu, S. Han, J. Wang, Y. Meng, Q. Xu, Y. Li, N. Chen, C. Zhang, Bioresour. Technol. 354 (2022) 127196.
[11] R. Fujiwara, S. Noda, T. Tanaka, A. Kondo, Nat. Commun. (2020) 279.
[12] M.T. Fernandez-Sandoval, J. Galindez-Mayer, F. Bolivar, G. Gosset, O.T. Ramirez, A. Martinez, Microb. Cell Factories 18 (2019) 145.
[13] R. Ledesma-Amaro, Z. Lazar, M. Rakicka, Z. Guo, F. Fouchard, A.-M.C.-L. Coq, J.-M. Nicaud, Metab. Eng. 38 (2016) 115–124.
[14] W. Wei, P. Zhang, Y. Shang, Y. Zhou, B.C. Ye, Bioresour. Technol. 314 (2020) 123726.
[15] N. Wei, E.J. Oh, G. Million, J.H. Cate, Y.S. Jin, ACS Synth. Biol. 4 (2015) 707–713.
[16] Y.J. Lee, P. Hoang Nguyen Tran, J.K. Ko, G. Gong, Y. Um, S.O. Han, S.M. Lee, Front. Bioeng. Biotechnol. 10 (2022) 826787.
[17] S.B. Lee, M. Tremaine, M. Place, L. Liu, A. Pier, D.J. Krause, D. Xie, Y. Zhang, R. Landick, A.P. Gasch, C.T. Hittinger, T.K. Sato, Metab. Eng. 68 (2021) 119–130.
[18] S. Watanabe, T. Kodaki, K. Makino, J. Biol. Chem. 280 (2005) 10340–10349.
[19] S. Watanabe, A.A. Saleh, S.P. Pack, N. Annaluru, T. Kodaki, K. Makino, J. Biotechnol. 130 (2007) 316–319.
[20] J.T. Cunha, P.O. Soares, A. Romani, J.M. Thevelein, L. Domingues, Biotechnol. Biofuels Bioprod. 12 (2019) 20.
[21] J.H. Bae, M.J. Kim, B.H. Sung, Y.S. Jin, J.H. Sohn, Biotechnol. Biofuels Bioprod. 14 (2021) 223.
[22] V. Endalur Gopinarayanan, N.U. Nair, Nat. Commun. 9 (2018) 1233.
[23] X. Li, Y. Wang, G. Li, Q. Liu, R. Pereira, Y. Chen, J. Nielsen, Nat. Catal. 4 (2021) 783–796.
[24] J. Shi, Y. Jiang, Z. Jiang, X. Wang, X. Wang, S. Zhang, P. Han, C. Yang, Chem. Soc. Rev. 44 (2015) 5981–6000.
[25] J. Li, J. Ren, S. Li, G. Li, M.M.-J. Li, R. Li, Y.S. Kang, X. Zou, Y. Luo, B. Liu, Y. Zhao, Green Energy Environ. (2023), https://doi.org/10.1016/j.gee.2023.05.003.
[26] H. Wang, Z. Liang, M. Tang, G. Chen, Y. Li, W. Chen, D. Lin, Z. Zhang, G. Zhou, J. Li, Z. Lu, K. Chan, T. Tan, Y. Cui, Joule 3 (2019) 1927–1936.
[27] X. Tan, J. Nielsen, Chem. Soc. Rev. 51 (2022) 4763–4785.
[28] M. Wang, Q. Zou, X. Dong, N. Xu, R. Shao, J. Ding, Y. Zhang, J. Qiao, Green Energy Environ. 8 (2023) 893–903.
[29] J. Li, Z. Zhang, W. Hu, Green Energy Environ. 7 (2022) 855–857.
[30] K. Wang, Y. Da, H. Bi, Y. Liu, B. Chen, M. Wang, Z. Liu, J. Nielsen, T. Tan, Renew. Energy 208 (2023) 331–340.
[31] O. Yishai, S.N. Lindner, J. Gonzalez De La Cruz, H. Tenenboim, A. Bar-Even, Curr. Opin. Chem. Biol. 35 (2016) 1–9.
[32] L. Calzadiaz-Ramirez, A.S. Meyer, Curr. Opin. Biotechnol. 73 (2022) 95–100.
[33] S. Kim, S.N. Lindner, S. Aslan, O. Yishai, S. Wenk, K. Schann, A. Bar-Even, Nat. Chem. Biol. 16 (2020) 538–545.

Please cite this article as: K. Wang et al., The transition from 2G to 3G-feedstocks enabled efficient production of fuels and chemicals, Green Energy & Environment, https://doi.org/10.1016/j.gee.2023.11.004

[34] O. Yishai, M. Bouzon, V. Döring, A. Bar-Even, ACS Synth. Biol. 7 (2018) 2023−2028.
[35] J. Bang, C.H. Hwang, J.H. Ahn, J.A. Lee, S.Y. Lee, Nat. Microbiol. 5 (2020) 1459−1463.
[36] R.A. Arkowitz, R.H. Abeles, Biochemistry 30 (1991) 4090−4097.
[37] S. Gleizer, R. Ben-Nissan, Y.M. Bar-On, N. Antonovsky, E. Noor, Y. Zohar, G. Jona, E. Krieger, M. Shamshoum, A. Bar-Even, R. Milo, Cell 179 (2019) 1255−1263 e1212.
[38] T. Gassler, M. Sauer, B. Gasser, M. Egermeier, C. Troyer, T. Causon, S. Hann, D. Mattanovich, M.G. Steiger, Nat. Biotechnol. 38 (2020) 210−216.
[39] Y. Zhang, J. Zhou, Y. Zhang, T. Liu, X. Lu, D. Men, X.E. Zhang, ACS Synth. Biol. 10 (2021) 707−715.
[40] B.M. Long, W.Y. Hee, R.E. Sharwood, B.D. Rae, S. Kaines, Y.L. Lim, N.D. Nguyen, B. Massey, S. Bala, S. Von Caemmerer, M.R. Badger, G.D. Price, Nat. Commun. 9 (2018) 3570.
[41] J.H. Park, D.H. Kim, H.S. Kim, G.F. Wells, H.D. Park, Bioresour. Technol. 281 (2019) 318−325.
[42] B. Endrodi, E. Kecsenovity, A. Samu, F. Darvas, R.V. Jones, V. Torok, A. Danyi, C. Janaky, ACS Energy Lett. 4 (2019) 1770−1777.
[43] F. Xia; J. Du; K. Wang; L. Liu; L. Ba; H. Liu; Y. Liu, 70 (2022) 11336-11343.
[44] Y.J. Zhou, N.A. Buijs, Z. Zhu, J. Qin, V. Siewers, J. Nielsen, Nat. Commun. 7 (2016) 11709.
[45] Y. Zhang, J. Wang, Z. Wang, Y. Zhang, S. Shi, J. Nielsen, Z. Liu, Nat. Commun. 10 (2019) 1053.
[46] Y. Zhang, M. Su, N. Qin, J. Nielsen, Z. Liu, Microb. Cell Factories 19 (2020) 226.
[47] K. Wang, Y. Liu, Z. Wu, Y. Wu, H. Bi, Y. Liu, M. Wang, B. Chen, J. Nielsen, Z. Liu, T. Tan, Green Carbon 1 (2023) 65−74.
[48] E. Fischer, N. Zamboni, U. Sauer, Anal. Biochem. 325 (2004) 308−316.
[49] C. Su, L. Qi, D. Cai, B. Chen, H. Chen, C. Zhang, Z. Si, Z. Wang, G. Li, P. Qin, Renew. Energy 162 (2020) 1125−1131.
[50] C. Su, C. Zhang, Y. Wu, Q. Zhu, J. Wen, Y. Wang, J. Zhao, Y. Liu, P. Qin, D. Cai, Renew. Energy 200 (2022) 592−600.
[51] H. Bi, C. Xv, C. Su, P. Feng, C. Zhang, M. Wang, Y. Fang, T. Tan, Fermentation 8 (2022) 532.
[52] S. Chen, Z. Xu, B. Ding, Y. Zhang, S. Liu, C. Cai, M. Li, B.E. Dale, M. Jin, Sci. Adv. 9 (2023) eadd8835.
[53] T.K. Sato, M. Tremaine, L.S. Parreiras, A.S. Hebert, K.S. Myers, A.J. Higbee, M. Sardi, S.J. Mcilwain, I.M. Ong, R.J. Breuer, R. Avanasi Narasimhan, M.A. Mcgee, Q. Dickinson, A. La Reau, D. Xie, M. Tian, J.L. Reed, Y. Zhang, J.J. Coon, C.T. Hittinger, A.P. Gasch, R. Landick, PLoS Genet. 12 (2016) e1006372.
[54] S.W. Jones, A.G. Fast, E.D. Carlson, C.A. Wiedel, J. Au, M.R. Antoniewicz, E.T. Papoutsakis, B.P. Tracy, Nat. Commun. 7 (2016) 12800.
[55] Y.J. Li, M.M. Wang, Y.W. Chen, M. Wang, L.H. Fan, T.W. Tan, Sci. Rep. 7 (2017) 43875.
[56] H. Moon, S. Kim, B.H. Jo, H.J. Cha, J. CO_2 Util. 39 (2020) 101172.
[57] C. Molina-Fernández, P. Luis, J. CO_2 Util. 47 (2021) 101475.
[58] T.G. Cooper, H.G. Wood, J. Biol. Chem. 246 (1971) 5488−5490.
[59] C. Zhan, X. Li, G. Lan, E.E.K. Baidoo, Y. Yang, Y. Liu, Y. Sun, S. Wang, Y. Wang, G. Wang, J. Nielsen, J.D. Keasling, Y. Chen, Z. Bai, Nat. Catal. 6 (2023) 435−450.
[60] K. Paramasivan, S. Mutturi, Crit. Rev. Biotechnol. 37 (2017) 974−989.
[61] Y. Cao, R. Zhang, W. Liu, G. Zhao, W. Niu, J. Guo, M. Xian, H. Liu, Sci. Rep. 9 (2019) 95.

Please cite this article as: K. Wang et al., The transition from 2G to 3G-feedstocks enabled efficient production of fuels and chemicals, Green Energy & Environment, https://doi.org/10.1016/j.gee.2023.11.004